# Stepping stone: a cytohesin adaptor for membrane cytoskeleton restraint in the syncytial *Drosophila* embryo

Jiangshu Liu[a], Donghoon M. Lee[a], Cao Guo Yu[a], Stephane Angers[b,c], and Tony J. C. Harris[a]
[a]Department of Cell and Systems Biology, [b]Department of Pharmaceutical Sciences, Leslie Dan Faculty of Pharmacy, and [c]Department of Biochemistry, University of Toronto, Toronto, ON M5S 3G5, Canada

**ABSTRACT** **Cytohesin Arf-GEFs are conserved plasma membrane regulators. The sole *Drosophila* cytohesin, Steppke, restrains Rho1-dependent membrane cytoskeleton activity at the base of plasma membrane furrows of the syncytial embryo. By mass spectrometry, we identified a single major Steppke-interacting protein from syncytial embryos, which we named Stepping stone (Sstn). By sequence, Sstn seems to be a divergent homologue of the mammalian cytohesin adaptor FRMD4A. Our experiments supported this relationship. Specifically, heterophilic coiled-coil interactions linked Sstn and Steppke in vivo and in vitro, whereas a separate C-terminal region was required for Sstn localization to furrows. Sstn mutant and RNAi embryos displayed abnormal, Rho1-dependent membrane cytoskeleton expansion from the base of pseudocleavage and cellularization furrows, closely mimicking Steppke loss-of-function embryos. Elevating Sstn furrow levels had no effect on the *steppke* phenotype, but elevating Steppke furrow levels reversed the *sstn* phenotype, suggesting that Steppke acts downstream of Sstn and that additional mechanisms can recruit Steppke to furrows. Finally, the coiled-coil domain of Steppke was required for Sstn binding and in addition homodimerization, and its removal disrupted Steppke furrow localization and activity in vivo. Overall we propose that Sstn acts as a cytohesin adaptor that promotes Steppke activity for localized membrane cytoskeleton restraint in the syncytial *Drosophila* embryo.**

**Monitoring Editor**
Richard Fehon
University of Chicago

Received: Nov 24, 2014
Revised: Dec 12, 2014
Accepted: Dec 15, 2014

## INTRODUCTION

Small G proteins are binary switches that control a wide range of cellular processes (Bos *et al.*, 2007; Cherfils and Zeghouf, 2013). Conversion to their active GTP-bound state is regulated in space and time by guanine nucleotide exchange factors (GEFs). A major question concerns how the GEFs are controlled. GEFs are typically multidomain proteins, and their recruitment by scaffold/adaptor proteins provides one regulatory mechanism. This mechanism is exemplified by Son-of-sevenless (Sos), a Ras-GEF that is recruited to receptor tyrosine kinases by the SH2-SH3 protein Grb2 (Bos *et al.*, 2007). Another example is that of G protein–coupled receptors, which, through the same polypeptide chain, connect reception of a ligand with GEF activity elsewhere in the protein (Rosenbaum *et al.*, 2009). Other than these paradigms, however, we have limited knowledge of scaffold/adaptor proteins that promote GEF activity.

Different small G protein families are regulated by structurally distinct families of GEFs (Bos *et al.*, 2007; Cherfils and Zeghouf, 2013). Our work focuses on Steppke (Step), the sole cytohesin family member in *Drosophila* (Gillingham and Munro, 2007). Cytohesins are composed of multiple domains (a coiled-coil [CC] domain, a Sec7 GEF domain, a PH domain, and a polybasic region) and activate plasma membrane Arf small G proteins (Gillingham and Munro, 2007). Plasma membrane Arf small G proteins are major inducers of endocytosis, lipid signaling, and actin remodeling, affecting a range of membrane complexes (D'Souza-Schorey and Chavrier, 2006; Gillingham and Munro, 2007; Donaldson and Jackson, 2011).

Thus far, several scaffold/adaptor proteins have been identified to link cytohesins to specific complexes. Connector Enhancer of KSR 1 (CNK1) binds cytohesins through their CC domain and

This article was published online ahead of print in MBoC in Press (http://www.molbiolcell.org/cgi/doi/10.1091/mbc.E14-11-1554) on December 24, 2014.

Address correspondence to: Tony J. C. Harris (tony.harris@utoronto.ca).

Abbreviations used: CC, coiled-coil; CNK1, Connector Enhancer of KSR 1; GEF, guanine nucleotide exchange factor; IP, immunoprecipitation; LC-MS, liquid chromatography mass spectrometry; mCh, mCherry; Sstn, Stepping stone; Step, Steppke.

recruits them to the plasma membrane in response to insulin signaling (Lim *et al.*, 2010). Myeloid-differentiation factor 88 (MYD-88) forms a complex with cytohesins for interleukin-1β signaling (Zhu *et al.*, 2012). Tamalin/GRP1-associated scaffold protein (GRASP) can recruit cytohesins to the plasma membrane (Nevrivy *et al.*, 2000) and mediates interactions with group 1 metabotropic glutamate receptors at synapses (Kitano *et al.*, 2002). Paxillin binds to cytohesins via their polybasic region and links them to focal adhesions at the leading edge of migratory cells (Torii *et al.*, 2010). FERM domain–containing 4A (FRMD4A) and GRP1-binding partner (GRSP-1) each bind to cytohesins through CC domain interactions and link them to Par-3 at adherens junctions (Ikenouchi and Umeda, 2010). These mammalian cell culture studies suggest that adaptor proteins couple cytohesins to specific complexes.

To test the generality and evolution of cytohesin adaptors, it is important to examine them in other animal models. For example, in *Drosophila*, Step regulates both insulin (Fuss *et al.*, 2006) and epidermal growth factor (Hahn *et al.*, 2013) signaling. Significantly, Step can bind *Drosophila* CNK and has been shown to interact genetically with the adaptor during epidermal growth factor–dependent patterning of the wing (Hahn *et al.*, 2013). Thus CNK may be commonly used to link cytohesins with receptor tyrosine kinase signaling pathways (Lim *et al.*, 2010; Hahn *et al.*, 2013).

In addition, Step functions to control plasma membrane growth in the early embryo (Lee and Harris, 2013). The early *Drosophila* embryo is a syncytium in which plasma membrane furrows transiently separate dividing peripheral nuclei and then cellularize ~6000 nuclei to form the cellular blastoderm (Lee and Harris, 2014). In this model of cell division, furrows normally extend straight down from the embryo surface plasma membrane and form a matrix of lateral membranes to separate nuclei. Without Step activity, the furrows extend into the embryo but then abnormally expand perpendicularly at their basal tips. Normally, these basal tips are maintained by actomyosin networks organized by Rho1 pathways. Without Step, these networks become overactive and drive the abnormal membrane expansion. As a result, basal cell membranes form prematurely and physically expel nuclei from the forming blastoderm. Normally, Step localizes at the basal tips of the furrows and uses its Arf-GEF activity to keep the membrane cytoskeleton in check (Lee and Harris, 2013).

We hypothesized that a specific cytohesin adaptor might aid Step for the restraint of the membrane cytoskeleton in the syncytial embryo. Of the known cytohesin adaptors, Myd88, CNK, and paxillin have annotated *Drosophila* homologues that are expressed in the syncytial embryo (FlyBase); Tamalin/GRASP has no annotated homologue, and the most similar *Drosophila* protein from BLAST searches (Short spindle 6) in not expressed in the syncytial embryo (FlyBase); in addition, FRMD4A and GRSP-1 have no significant sequence similarities with *Drosophila* proteins (using BLAST searches), with the exception of their FERM domains, which most closely resemble the FERM domain of moesin. With these candidates in mind, we took a nonbiased approach to identify Step complex components of the syncytial embryo by liquid chromatography mass spectrometry (LC-MS). Our analyses identified one major interacting protein, which we named Stepping stone (Sstn). Despite substantial sequence divergence, Sstn appears to be a structural and functional homologue of FRMD4A and aids Step in the restraint of the membrane cytoskeleton.

## RESULTS

### Sstn is a major Step-interacting protein in syncytial embryos

To identify proteins that form complexes with Step in the syncytial *Drosophila* embryo, we expressed green fluorescent protein (GFP)–Step maternally, collected embryos undergoing peripheral syncytial divisions and cellularization, performed GFP immunoprecipitations (IPs), and identified precipitated *Drosophila* proteins by LC-MS. GFP-Step IPs were compared with GFP IPs to control for nonspecific precipitations.

GFP-Step IPs reproducibly contained only one other major protein, in addition to Step, that was not found in the control GFP IPs. A protein encoded by the uncharacterized gene CG6945 was repeatedly the protein with the greatest peptide counts in GFP-Step IPs (Table 1). Because it was the sole major protein isolated in the GFP-Step IPs, the interaction seemed to occur without an intermediary protein and was thus likely direct. As explained later, we renamed CG6945 *stepping stone* (*sstn*).

To confirm the interaction between Step and Sstn by LC-MS, we made a GFP-Sstn construct, expressed it, and immunoprecipitated it from early embryos. Endogenous Step was reproducibly the most abundant protein, other than Sstn, in these GFP-Sstn IPs not found in the control GFP IPs (Table 1). Moreover, IPs targeting GFP-Sstn from embryos co-overexpressing mCherry (mCh)-Step also identified Sstn and Step, each with much higher peptide counts than any other protein specifically precipitated in the sample (Table 1). The abundance of Step in the Sstn IPs further argued that their interaction was direct.

### Sequence analyses suggest that Sstn is a divergent homologue of FRMD4A

To assess the properties of the Sstn, we conducted sequence analyses. The protein contained a predicted CC domain in its N-terminal region but had no other predicted domains (Figure 1A). BLAST searches identified a C-terminal conserved region (CR) with high identity to sequences in a number of predicted insect proteins (Figure 1, A–C). Bioinformatic analyses of these proteins revealed that they also contain a predicted N-terminal CC domain (Figure 1A). Moreover, the proteins from monarch butterflies (*Danaus plexippus*) and leaf-cutter ants (*Acromyrmex echinatior*) were previously annotated as FRMD4A-like proteins, although they lack the FERM domain of FRMD4A. For these proteins, our BLAST analyses revealed that their top *Drosophila* hit was Sstn, whereas their top human hit was a predicted FRMD4A isoform (Figure 1B). Their similarity with Sstn occurs in the CR, as mentioned, but their similarity with human FRMD4A occurs within their CC domains (color coding in Figure 1B).

FRMD4A contains a FERM domain followed by a CC domain and a long C-terminus with no clear domains (Ikenouchi and Umeda, 2010). C-terminal to the FERM domain of FRMD4A, the domain organization and overall length of the protein were similar to those of Sstn and its insect homologues (Figure 1A). Multiple alignments of the CC domains and CRs revealed similarities across the species consistent with Sstn being a divergent homologue of human FRMD4A (Figure 1C). Although neither Sstn nor human FRMD4A was hit in each other's BLAST searches (Figure 1B), no other proteins were clear homologues in either species. Because Sstn lacks a FERM domain, naming it FRMD4A-like would be a misnomer. Thus we named it Stepping stone for its interaction with Step and its loss-of-function phenotype described later.

### Sstn and Step interact directly through their coiled-coil domains in vitro

The CC domain of FRMD4A binds to the CC domains of cytohesins (Ikenouchi and Umeda, 2010). If Sstn is a homologue of FRMD4A, a similar interaction with Step would be expected. Our IP-MS data implicated a direct Sstn–Step interaction. To test further for the

| | IP target[a] | | | | IP target | | | | | |
|---|---|---|---|---|---|---|---|---|---|---|
| | GFP-Step | | | | GFP-Sstn | | | GFP-Sstn[b] | | |
| LC-MS hits[c] | R1 | R2 | R3 | LC-MS hits[c] | R1 | R2 | R3 | R1 | R2 | R3 |
| Step | 52 | 33 | 64 | Sstn | 122 | 137 | 96 | 345 | 171 | 145 |
| Sstn/CG6945 | 7 | 3 | 17 | Step | 32 | 23 | 31 | 424 | 190 | 214 |
| Fer2LCH | 1 | 2 | 2 | smg | 6 | 13 | 17 | 5 | 2 | 2 |
| | | | | Ranbp9 | 8 | 14 | 12 | 3 | 3 | 1 |
| | | | | rod | 7 | 12 | 5 | 3 | 2 | 1 |
| | | | | cnn | 12 | 2 | 6 | 0 | 0 | 0 |
| | | | | pxt | 7 | 7 | 8 | 3 | 3 | 0 |
| | | | | Ca-P60A | 7 | 8 | 4 | 3 | 1 | 0 |
| | | | | eIF4G | 6 | 7 | 6 | 2 | 1 | 2 |
| | | | | Mpcp | 4 | 4 | 4 | 0 | 0 | 0 |
| | | | | faf | 3 | 2 | 5 | 0 | 2 | 1 |
| | | | | pen | 3 | 2 | 5 | 2 | 2 | 0 |
| | | | | Cand1 | 4 | 3 | 4 | 0 | 1 | 0 |
| | | | | mts | 2 | 4 | 3 | 1 | 2 | 0 |
| | | | | cup | 1 | 4 | 7 | 2 | 0 | 0 |
| | | | | lost | 3 | 1 | 4 | 1 | 0 | 0 |
| | | | | brat | 1 | 5 | 1 | 0 | 0 | 0 |

[a]Targets were expressed from UAS-transgenes maternally with the mgv driver.
[b]GFP-Sstn coexpressed with mCh-Step (note the gain of Sstn and Step peptides and the loss of peptides for proteins precipitated with GFP-Sstn when expressed alone).
[c]All proteins detected in each of three replicates (R1–R3) but not in GFP IP controls.

**TABLE 1:** LC-MS peptide counts for proteins reproducibly and specifically in GFP-Step or GFP-Sstn IPs from syncytial embryos.

interaction and map the sequences involved, we designed full-length and deletion constructs for Sstn and Step (Figure 2A), purified the proteins from bacteria, and pursued blot overlays. Maltose-binding protein (MBP)–Sstn was separated by SDS–PAGE, blotted, and then probed with purified glutathione *S*-transferase (GST)–Step, followed by GST antibodies. A very strong signal for GST-Step was detected where major proteolytic fragments of the MBP-Sstn protein were positioned on the blot (Figure 2B). Slightly higher levels of GST showed no binding to MBP-Sstn, and slightly higher levels of MBP showed no binding to GST-Step (Figure 2B). Thus Sstn and Step can interact directly in vitro, and the interacting MBP-Sstn fragment sizes suggested that the interaction site was in the N-terminal half of Sstn.

Because the Sstn–Step interaction seemed to occur through the N-terminal half of Sstn, we pursued the CC domains by deleting them from both Sstn and Step. The GST-Step interaction with MBP-Sstn was abolished when the CC domains were deleted from either MBP-Sstn or GST-Step, despite higher amounts of the deletion constructs in the assays (Figure 2B). Thus, similar to FRMD4A and cytohesins (Ikenouchi and Umeda, 2010), both Sstn and Step require their CC domains for direct interaction in vitro.

### The Sstn coiled-coil domain and conserved region have separate interactions in vivo

If Sstn acts as a cytohesin adaptor, then one region of the protein would be expected to bind Step, and a separate region would be expected mediate other interactions. To test this hypothesis, we generated GFP-tagged versions of Sstn, expressed them from the same genomic site with the Gal-4-UAS system, and localized them in the early embryo during peripheral nuclear divisions and early cellularization. Full-length Sstn accumulated at two main sites within the cell compartments: to pericentrosomal regions and along the basal end of pseudocleavage and early cellularization furrows (Figure 3A; arrow at basal furrow tip). We attempted to generate antibodies against both the CC domain and the CR of Sstn, but neither detected Sstn specifically in early embryos.

To test the role of the CC domain and CR in this localization pattern, we analyzed the constructs with each region removed. Deletion of the CC domain had no apparent effect on localization to the base of furrows but did lead to a reduction of pericentrosomal localization and an increase in the cytoplasmic pool (Figure 3A; arrow at basal furrow tip). Deletion of the CR strongly reduced localization to the base of the furrows and also decreased pericentrosomal accumulation but without apparent increases to the cytoplasmic pool (Figure 3A). Quantifications confirmed a statistically significant reduction of furrow base protein levels for GFP-Sstn$^{\Delta CR}$ versus GFP-Sstn or GFP-Sstn$^{\Delta CC}$, which were indistinguishable (Figure 3B). In addition, we performed line scans from centrosomes to basal furrow tips and found that for embryos with similar centrosome protein levels, the furrow protein levels of GFP-Sstn$^{\Delta CR}$ were indistinguishable from cytosolic protein levels, in contrast to GFP-Sstn or GFP-Sstn$^{\Delta CC}$, which accumulated at furrows (Figure 3C). Thus Sstn associations with the basal end of furrows require the CR but occur without the CC domain. Of note, both regions were needed for full centrosome association.

To determine the relationship between Step and the different pools of Sstn, we conducted co-overexpression experiments. Coexpression of GFP-Sstn with mCh-Step induced greater furrow levels

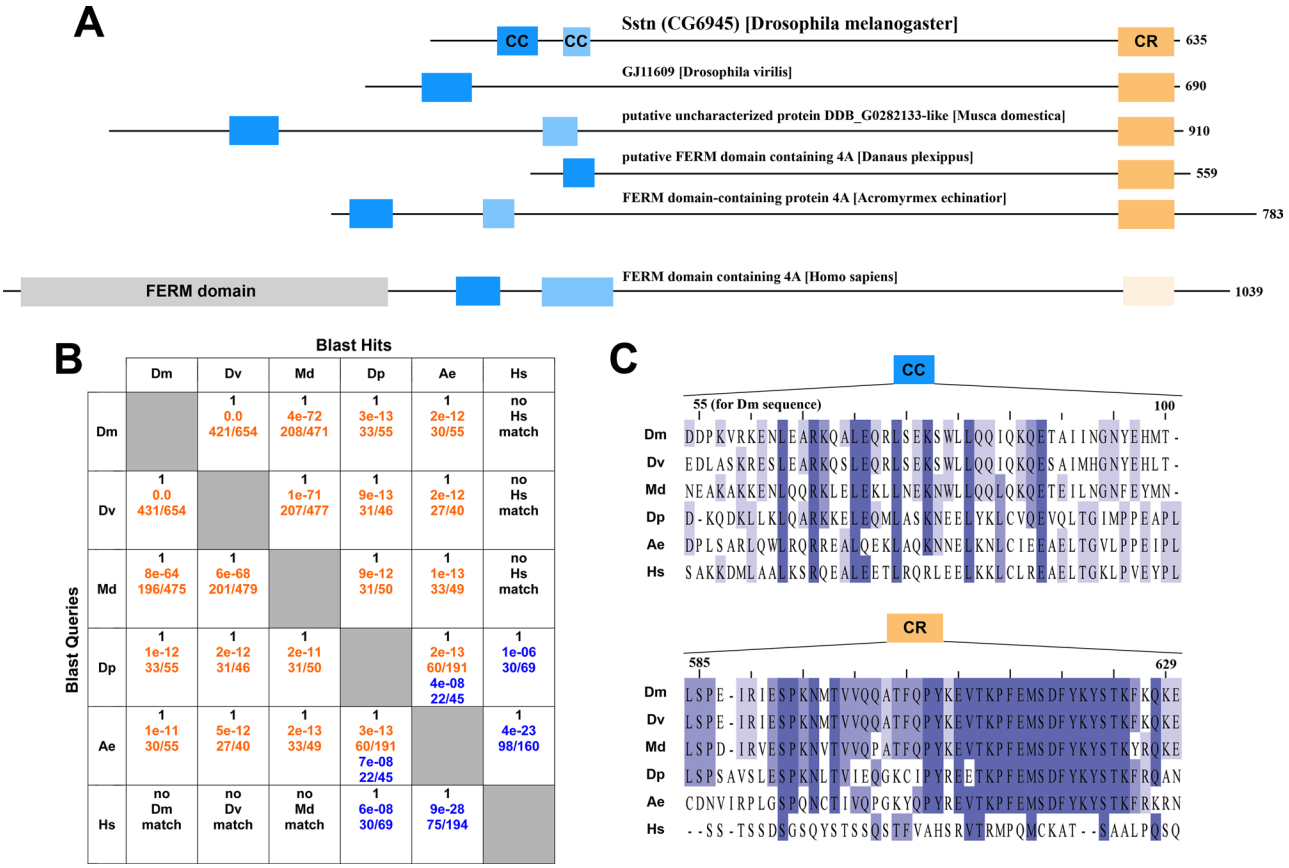


| Blast Queries | Dm | Dv | Md | Dp | Ae | Hs |
|---|---|---|---|---|---|---|
| Dm | | 1<br>0.0<br>421/654 | 1<br>4e-72<br>208/471 | 1<br>3e-13<br>33/55 | 1<br>2e-12<br>30/55 | no<br>Hs<br>match |
| Dv | 1<br>0.0<br>431/654 | | 1<br>1e-71<br>207/477 | 1<br>9e-13<br>31/46 | 1<br>2e-12<br>27/40 | no<br>Hs<br>match |
| Md | 1<br>8e-64<br>196/475 | 1<br>6e-68<br>201/479 | | 1<br>9e-12<br>31/50 | 1<br>1e-13<br>33/49 | no<br>Hs<br>match |
| Dp | 1<br>1e-12<br>33/55 | 1<br>2e-12<br>31/46 | 1<br>2e-11<br>31/50 | | 1<br>2e-13<br>60/191<br>4e-08<br>22/45 | 1<br>1e-06<br>30/69 |
| Ae | 1<br>1e-11<br>30/55 | 1<br>5e-12<br>27/40 | 1<br>2e-13<br>33/49 | 1<br>3e-13<br>60/191<br>7e-08<br>22/45 | | 1<br>4e-23<br>98/160 |
| Hs | no<br>Dm<br>match | no<br>Dv<br>match | no<br>Md<br>match | 1<br>6e-08<br>30/69 | 1<br>9e-28<br>75/194 | |

FIGURE 1: Sequences analyses place Sstn within a conserved group of insect proteins with similarity to human FRMD4A. (A) Predicted domain structures of Sstn (CG6945) and similar proteins in other insects and humans: CC; coiled-coil; CR conserved region. (B) Matrix of blastp results. Blast queries (the proteins shown in A) are listed in the first column. The following columns show the blast hits in the other species, with the rank of the match among other proteins in the species (all are the top-ranked match in other species: 1), the expected score for the match, and the identical residues over the total residues in the blast result. Matches centered on the CC domain and CR are shown in orange and blue, respectively. (C) Multiple alignments of the CC domain and CR for the proteins shown in A. Note the high sequence identity for the CR among all of the insect species (Dm, Dv, Md, Dp, and Ae). Note the high sequence identity for the CC domains of butterfly (Dp), ant (Ae), and human (Hs) and the high sequence identity for the CC domains of *Drosophila* species (Dm and Dv) and house fly (Md).

for each protein versus single-overexpression controls (Figure 4A; statistical significance shown with quantifications at right), and the proteins colocalized at the membranes. mCh-Step solely localized to the plasma membrane regardless of Sstn coexpression, but the increase in Sstn furrow localization coincided with a decrease in centrosome localization (Figure 4A; line scans from embryos with similar furrow protein levels show the reproducible effect on the centrosome-associated pool). Of interest, the displacement of Sstn from centrosomes was also evident in our proteomic analyses, as centrosomin reproducibly precipitated with GFP-Sstn when expressed alone but not when coexpressed with mCh-Step (Table 1). Thus Sstn-Step associations seem to occur preferentially at plasma membrane furrows.

Because Sstn and Step supported each other's furrow localization when overexpressed, we used this behavior as an assay to determine the sequence dependence of their association at furrows. Coexpression of GFP-Sstn$^{\Delta CC}$ and mCh-Step failed to increase the furrow levels of either protein, indicating that the mutually supportive Sstn–Step interactions were dependent on the CC domain of Sstn (Figure 4B). In fact, mCh-Step coexpression led to a reduction of GFP-Sstn$^{\Delta CC}$ versus its single overexpression, but this change did not affect the centrosome:furrow ratio of GFP-Sstn$^{\Delta CC}$ (Figure 4B). Coexpression of GFP-Sstn$^{\Delta CR}$ and mCh-Step led to increased furrow levels and colocalization of each protein (Figure 4C), indicating that the mutually supportive Sstn–Step interactions were independent of the CR of Sstn. To investigate whether the increases to furrow protein levels were associated with the formation of physical complexes, we performed IP experiments from embryos coexpressing the GFP-Sstn and mCh-Step constructs. IPs of GFP-Sstn and GFP-Sstn$^{\Delta CR}$ strongly precipitated mCh-Step, but IPs of GFP-Sstn$^{\Delta CC}$ did not (despite similar IPs of each GFP-Sstn protein and similar mCh-Step protein levels available in each lysate; Figure 4D). Together these data confirm that the Sstn CC domain interacts with Step in vivo and that Sstn and Step can use the CC domain to elevate each other's abundance at plasma membrane furrows of the syncytial embryo.

Overall these overexpression studies revealed two separate interactions mediated by the two distinctive regions of Sstn. The CC domain interacted with Step but was not needed for membrane association, whereas the CR-mediated membrane associations had independence from Step. Step interaction and membrane association were not entirely separable, however, as evident from the membrane increase of GFP-Sstn$^{\Delta CR}$ with mCh-Step coexpression, and

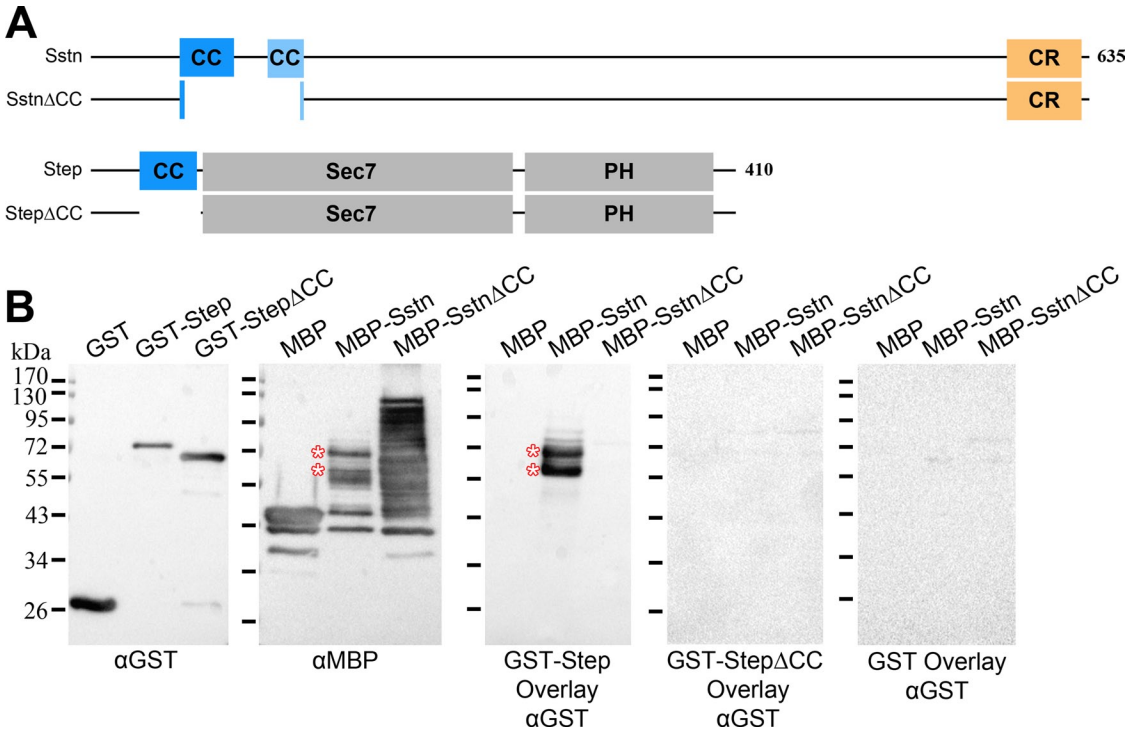


FIGURE 2: Mapping a direct interaction between the coiled-coil domains of Sstn and Step. (A) Sstn and Step constructs used in the binding assays. (B) Blot overlays showing binding of GST-Step to major MBP-Sstn proteolytic fragments (asterisks) but not to higher levels of MBP or MBP-Sstn$^{\Delta CC}$ fragments. GST and GST-Step$^{\Delta CC}$ showed no binding to the MBP-Sstn proteolytic fragments, despite incubation at higher levels than GST-Step (see left blot for the relative GST, GST-Step, and GST-Step$^{\Delta CC}$ protein levels used for the overlays shown). The overlay blots were probed and imaged side by side with identical reagents and settings. The overall results were replicated in a separate complete analysis.

thus other membrane association mechanisms may occur. Nonetheless, the basic properties of Sstn revealed by these experiments are consistent with it being a Step adaptor.

### Sstn loss leads to abnormal membrane cytoskeleton expansion

If Sstn contributes positively to Step activity, then removal of Sstn should result in the membrane cytoskeleton expansion defect that occurs with Step loss (Lee and Harris, 2013). To test the function of Sstn in vivo, we generated three *sstn* short hairpin RNA (shRNA) constructs unique to distinct sequences in *sstn* and acquired available *sstn* P-element insertions and deletions (Supplemental Figure S1). Maternal expression of the *sstn* shRNA constructs effectively depleted GFP-Sstn (Supplemental Figure S2) and led to the same specific change to the plasma membrane furrows of the early embryo. Both pseudocleavage and cellularization furrows extended effectively into the embryo, but, in contrast to controls, they then underwent abnormal perpendicular expansion at their basal tips (in embryo surface views, the nuclear spaces gained the appearance of stepping stones more widely separated across a pond; Figure 5A, quantified in Figure 5B; pseudocleavage furrows shown in Supplemental Figure S3). The expanded membranes were coated with a cytoskeleton marker (the septin Peanut) and were observed to encroach into space normally occupied by nuclei, resulting in nuclear indentations and bottle-like shapes (Supplemental Figure S4). The pseudocleavage and cellularization furrow defects also occurred in progeny of mothers transheterozygous for a *sstn* promoter P-element insertion and a large deletion removing *sstn* (quantified in Figure 5B; pseudocleavage furrows shown in Supplemental Figure S3) and for the *sstn* promoter P-element insertion and an *sstn* exon P-element insertion (unpublished data). These defects were very similar to, although somewhat milder than, those observed with Step loss (Lee and Harris, 2013). In addition, we observed preadult lethality of zygotic mutants transheterozygous for the large deletion and the *sstn* exon P-element insertion, indicating that Sstn functions in later development as well.

### Reduced Rho1 activity suppresses the effects of Sstn loss

The abnormal membrane expansion of *step* loss-of-function embryos was shown to be the result of Rho1 pathway and actomyosin overactivity through suppression experiments (Lee and Harris, 2013). To determine whether the abnormal membrane expansion of *sstn* loss-of-function embryos was due to similar misregulation, we reduced Rho1 pathway activity through *rho1* mutant heterozygosity, as done previously (Lee and Harris, 2013). Maternal heterozygosity for *rho1*$^{72O}$ substantially suppressed the *sstn* RNAi phenotype versus offspring of sibling mothers without the *rho1* reduction (Figure 6A; quantified in Figure 6B). Thus Sstn seems to antagonize effects of the Rho1 pathway in a manner very similar to that of Step.

### Step overexpression suppresses the effects of Sstn loss but not vice versa

To investigate the pathway relationship between Sstn and Step, we tested how they affect each other's localization and RNA interference (RNAi) phenotypes. For GFP-Sstn, we observed similar local levels of the protein at the base of furrows in control embryos and in *step* RNAi embryos with abnormal perpendicular expansion of furrow tips (Figure 7A). Thus it seems that Step is not essential for the localization of overexpressed Sstn. Moreover, the Sstn overexpression could not overcome the effects of Step loss. Sstn overexpression also had

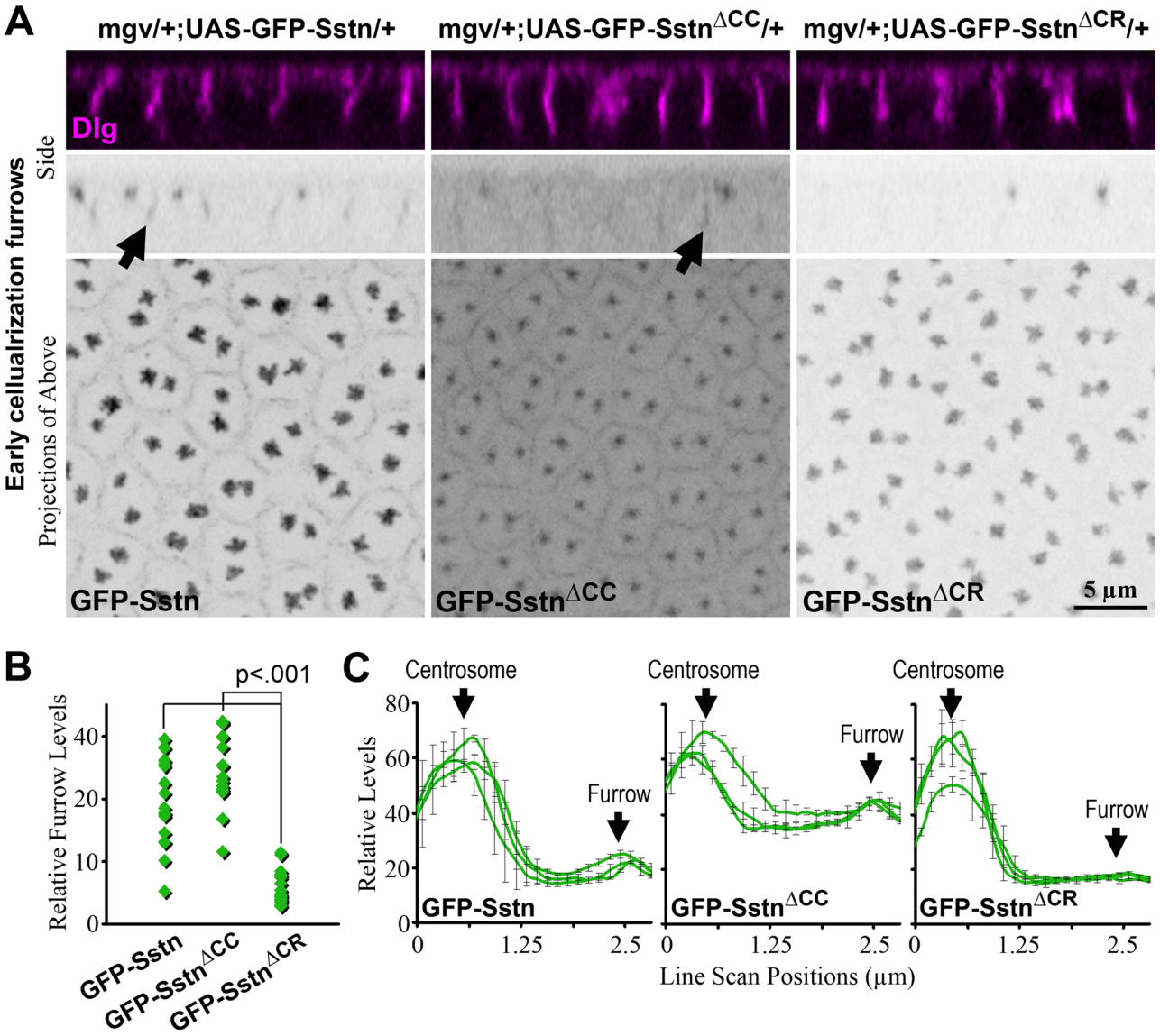


FIGURE 3: The Sstn coiled-coil domain and conserved region have distinct effects on subcellular localization. (A) Images of GFP-Sstn constructs acquired and adjusted with the same settings. Dlg staining shows cellularization furrows of similar depths. GFP-Sstn and Sstn$^{\Delta CC}$ are enriched at the base of furrows (arrows). All three constructs localize around the centrosomes (two per cell). (B) Quantifications of construct signals at the base of furrows. Each point is an average of five background corrected measurements from one confocal section of one cellularizing embryo with 2- to 5-µm-deep furrows. Results are shown from one set of crosses, and the overall results were reproduced with an independent set of crosses. (C) Quantifications of construct signal along lines from the centrosome to the furrow. Each curve represents the mean ± SD of three line scans with a similar spacing of centrosome and furrow in a single section from one embryo. To illustrate differences in furrow and cytosolic levels, three embryos with similar centrosome intensity are shown for each construct. The overall relationships were reproduced with an independent set of crosses.

no noticeable effect on otherwise genetically wild-type syncytial embryos.

To probe how Sstn affects Step localization, we first tested a characterized Step antibody (Hahn *et al.*, 2013). Despite specific detection of Step in later embryos (unpublished data) and larval tissues (Hahn *et al.*, 2013), we were unable to detect any signal above background in syncytial embryos (unpublished data). Thus endogenous Step seems to be present at relatively low levels at this stage. To examine higher levels of Step, we analyzed overexpressed GFP-Step. GFP-Step displayed similar local levels at the base of furrows in both control and *sstn* RNAi embryos (Figure 7B). Moreover, the overexpressed GFP-Step reduced the abnormal furrow expansion that otherwise occurs with *sstn* RNAi (Figure 7C). GFP-Step overexpression alone leads to GEF activity–dependent, sporadic furrow loss (presumably through weakening of the membrane cytoskeleton; Lee and Harris, 2013), and the embryos with both Sstn RNAi and Step overexpression resembled those with Step overexpression alone (Figure 7C, arrows; 22 of 52 and 15 of 27 early-cellularization embryos displayed sporadic missing furrows, respectively). These data indicate that when overexpressed, Step does not depend on *sstn* for its localization and that Step overexpression can overcome the effects of Sstn loss. Together these analyses implicate additional mechanisms for

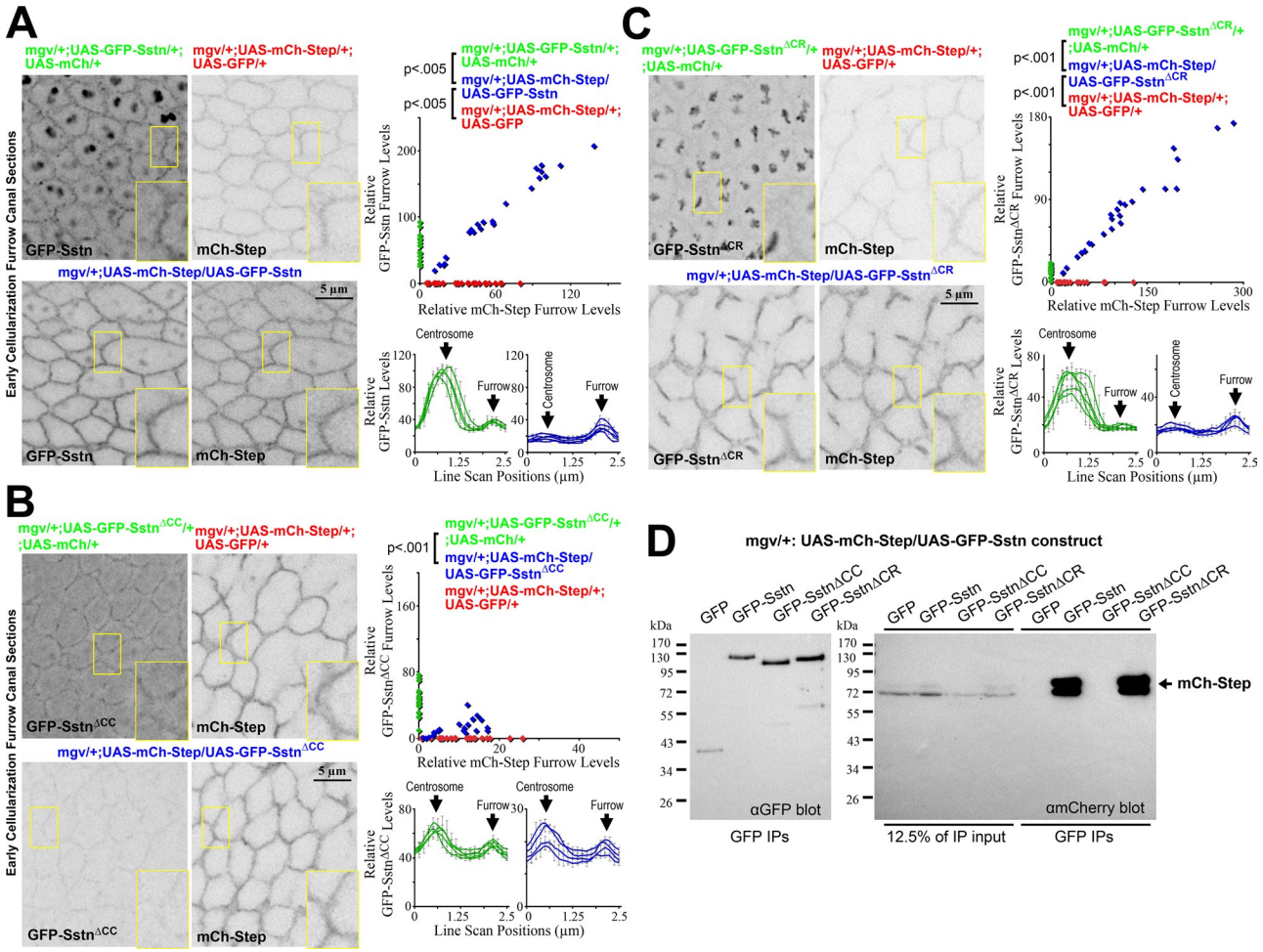


FIGURE 4: The Sstn and Step coiled-coil domains are needed for their interaction in vivo. (A–C) Furrow corecruitment of mCh-Step with GFP-Sstn (A) and GFP-Sstn$^{\Delta CR}$ (C) but not GFP-Sstn$^{\Delta CC}$ (B). In each case, images are shown after acquisition and adjustment with the same settings. Furrow levels were quantified as in Figure 3B, with GFP-Sstn construct levels on the *y*-axis and mCh-Step levels on the *x*-axis (the extension of the signal distributions with coexpression [blue points] beyond single-expression controls [green or red points] indicates corecruitment [each point is one embryo quantification]). Line scans were performed as in Figure 3C (each line is one embryo quantification). The overall relationships were reproduced with an independent set of crosses. (D) Co-IPs of mCh-Step with GFP-Sstn and GFP-Sstn$^{\Delta CR}$, but not GFP-Sstn$^{\Delta CC}$, from 0.5- to 2.5-h embryo lysates. The results were reproduced with an independent set of crosses.

localizing Sstn and Step and that Step likely acts downstream of Sstn in the membrane cytoskeleton restraint pathway.

### The Step coiled-coil domain affects Step localization and activity and mediates at least two different protein interactions

Because we found that the Sstn–Step interaction required the CC domains of each protein, we performed a final set of in vivo experiments interrogating the CC domain of Step. Specifically, we compared GFP-Step with a derivative in which the CC domain was deleted, expressing them from the same genomic site with the Gal-4-UAS system. First, we assessed in vivo associations with a mCh-tagged Sstn construct. Coexpression of GFP-Step with mCh-Sstn led to increased furrow abundance of both proteins versus single-expression controls (Figure 8A), as observed for proteins with the reciprocal tags (Figure 4A). In contrast, coexpression of GFP-Step$^{\Delta CC}$ with mCh-Sstn did not enhance the furrow level of either protein (Figure 8A).

To assess how deletion of CC domain affected the Step construct itself, we first compared its localization versus full-length Step. Full-length GFP-Step was enriched at the base of furrows (Figure 8B, arrow), as reported previously (Lee and Harris, 2013), but this enrichment was lost with GFP-Step$^{\Delta CC}$ (Figure 8B, arrow). Next we compared the activity of RNAi-resistant forms of each construct in embryos with coexpressed *step* shRNA. GFP-Step restrained the membrane cytoskeleton at furrow tips in this context, but GFP-Step$^{\Delta CC}$ was significantly less effective, as observed by basal membrane expansion into space normally occupied by nuclei (Figure 8C).

Together these data indicated that the Step CC domain was required for Sstn association, Step localization, and membrane cytoskeleton restraint. However, it seemed that the lack of Sstn association could not solely explain the effects of deleting the CC domain from Step. Specifically, GFP-Step localization and function were disrupted with deletion of the CC domain, but GFP-Step could localize and function with the depletion of Sstn. One explanation for

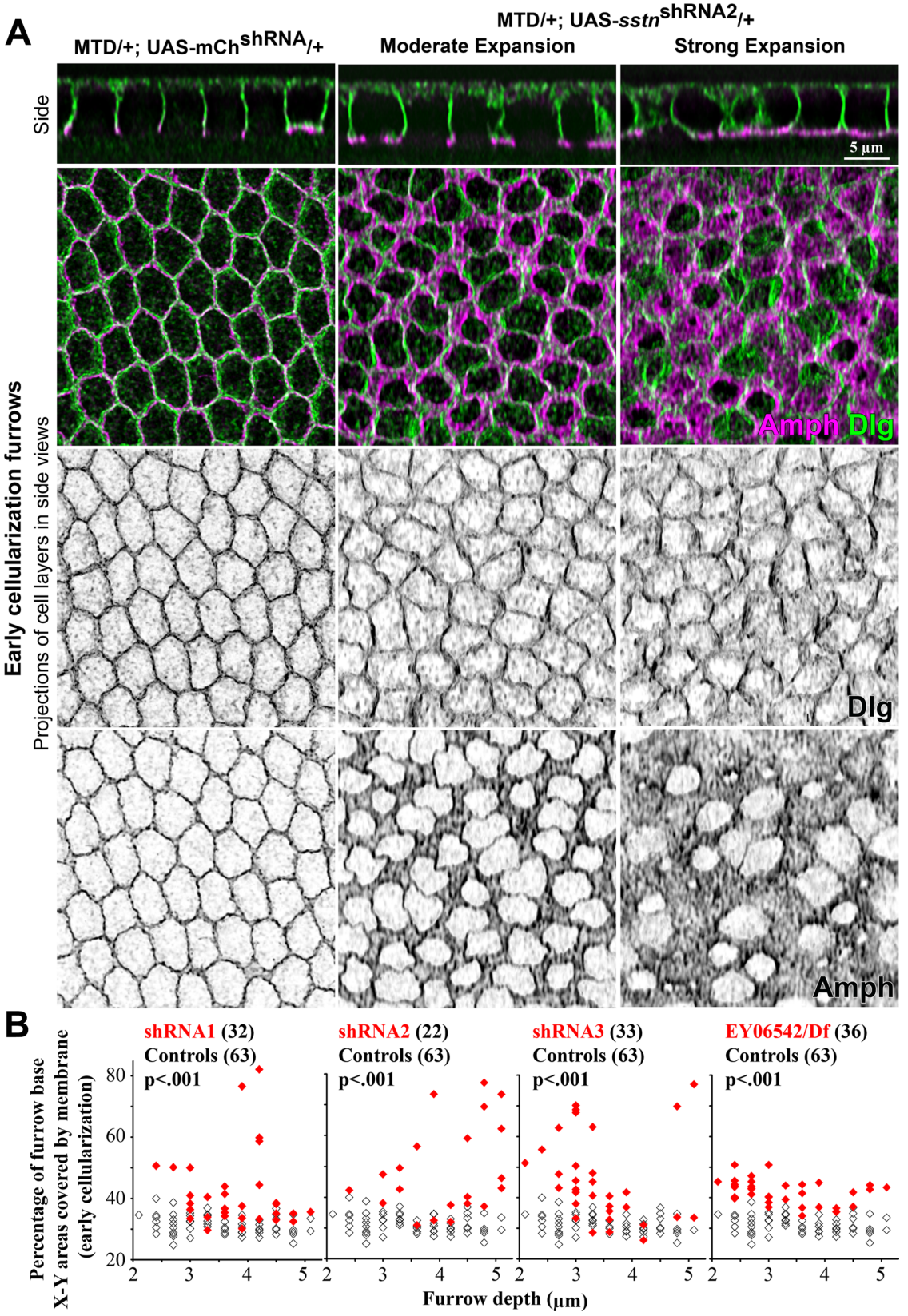


FIGURE 5: With Sstn loss membranes expand perpendicularly from the base of furrows. (A) Normal early-cellularization furrow organization with a control shRNA construct and perpendicular expansions of furrow bases with *sstn* shRNA. Disks large (Dlg) is enriched at lateral membranes, and amphiphysin (Amph) is enriched at the furrow base (the furrow canal). Note that the upper furrows stained with Dlg are minimally affected and that the membrane expansion occurs from the furrow base (seen with Amph). Embryos with moderate and strong membrane expansion are shown. Images were deconvolved. (B) Quantifications of furrow base areas (in *xy*-sections) for control; *sstn* shRNA and *sstn* mutant

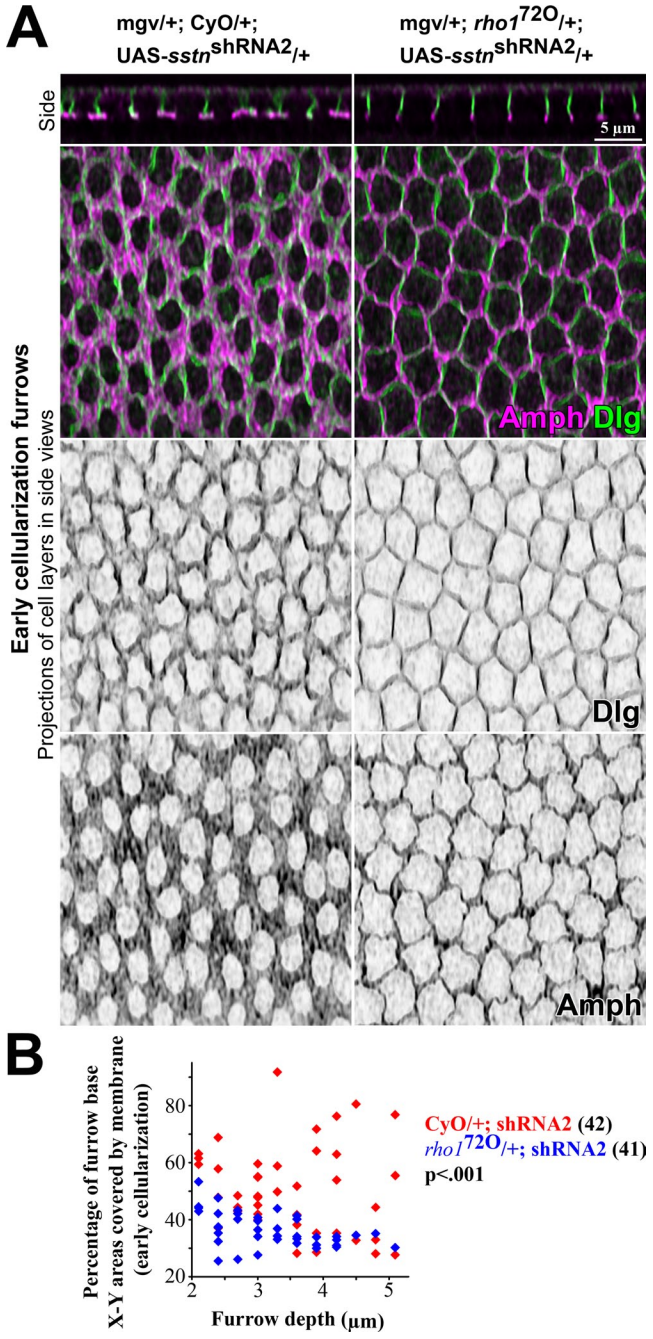


FIGURE 6: The membrane expansion with Sstn loss is due to Rho1 activity. (A) Suppression of the *sstn* shRNA membrane defect by reducing maternal Rho1 levels in half with heterozygosity for a null *rho1* allele but not in siblings heterozygous for a balancer chromosome. Images were deconvolved. (B) Quantification as in Figure 5.

this discrepancy would be additional interactions promoted by the Step CC domain. Suggesting one possible interaction, the CC domains of mammalian cytohesins have been shown to homodimerize (DiNitto *et al.*, 2007, 2010). To test for such homodimerization for Step, we purified bacterially expressed Step proteins with or without the CC domain. Using blot overlays, we detected Step–Step dimerization dependent on the CC domain (Figure 9). If this Step dimerization occurs in vivo, then the CC domain of Step may have two roles at plasma membranes: 1) direct interaction with Sstn and 2) indirect promotion of other membrane interactions through avidity effects with dimerization (see *Discussion*).

## DISCUSSION

Our data argue that an adaptor–Arf-GEF pair first identified in mouse cell culture (Ikenouchi and Umeda, 2010) is conserved and functional in *Drosophila*. Although the sequence similarity between mammalian FRMD4A and *Drosophila* Sstn is low, their relationship is supported by a range of data: 1) they share the same unique homologues in other species, 2) they lack similarity with any other proteins in mammals or *Drosophila*, 3) with the exception of the FERM domain, they share a common domain organization, 4) they both interact directly with cytohesins through CC domain heterodimerization, 5) they both colocalize with cytohesins in cells, and 6) they both promote cytohesin-dependent cellular processes.

In the early *Drosophila* embryo, our data suggest that Sstn supports the activity of the cytohesin homologue Step for the local control of plasma membrane growth. Specifically, Sstn localizes at the base of both pseudocleavage and cellularization furrows, where it appears to engage Step through direct interactions to keep the membrane cytoskeleton in check. Without Sstn, the basal tips of the furrows expand perpendicularly in a Rho1-dependent process that leads to abnormal plasma membrane encroachment into space normally occupied by nuclei of the forming cells. This misregulation is strikingly similar to that of *step* loss-of-function embryos (Lee and Harris, 2013). Moreover, it could be overcome by Step overexpression, suggesting that Sstn normally acts by enhancing the activity of a limited supply of endogenous Step. Thus we propose a model in which a Sstn–Step–Arf small G protein axis acts at the base of furrows to control their growth (Figure 10). Within this axis, Sstn and Step interact directly through their CC domains, but each also has independent interactions with other membrane components, mediated by the CR in the case of Sstn. Our data suggest that the Sstn–Step interaction may stabilize Step furrow localization, where Step has been shown to use its Arf-GEF activity to control membrane growth (Lee and Harris, 2013).

From our model, we propose that Sstn acts as an adaptor to link Step to specific targets for the local endocytic regulation of furrow tips. Our Sstn structure–function analysis shows that its C-terminal CR is critical for recruiting it to the plasma membrane, whereas its N-terminal CC domain is responsible for interacting with Step. We propose that the CR interacts with targets linked to the membrane cytoskeleton and that Sstn recruits Step for Arf small G protein activation, the induction of local endocytosis, and downstream antagonism of the membrane cytoskeleton. However, our mass spectrometry experiments did not identify any cytoskeletal proteins as partners of Sstn. Thus, in our model of Sstn as a cytohesin adaptor, it is unknown what targets Sstn bridges to Step. We speculate that the failure to identify these proteins may be related to their transient associations with Sstn as part of the proposed endocytosis pathway. For mouse FRMD4A, an interaction with cytohesins at its CC domain

cellularization embryos with 2- to 5.5-µm-deep furrows. In *xy* images of furrow bases, the percentage of total area occupied by Amph signal was calculated (Lee and Harris, 2013). The control data in each graph are a compilation of data from mCh shRNA embryos and Histone-GFP embryos collected across the experiments. Each point is from one embryo (total embryo numbers bracketed).

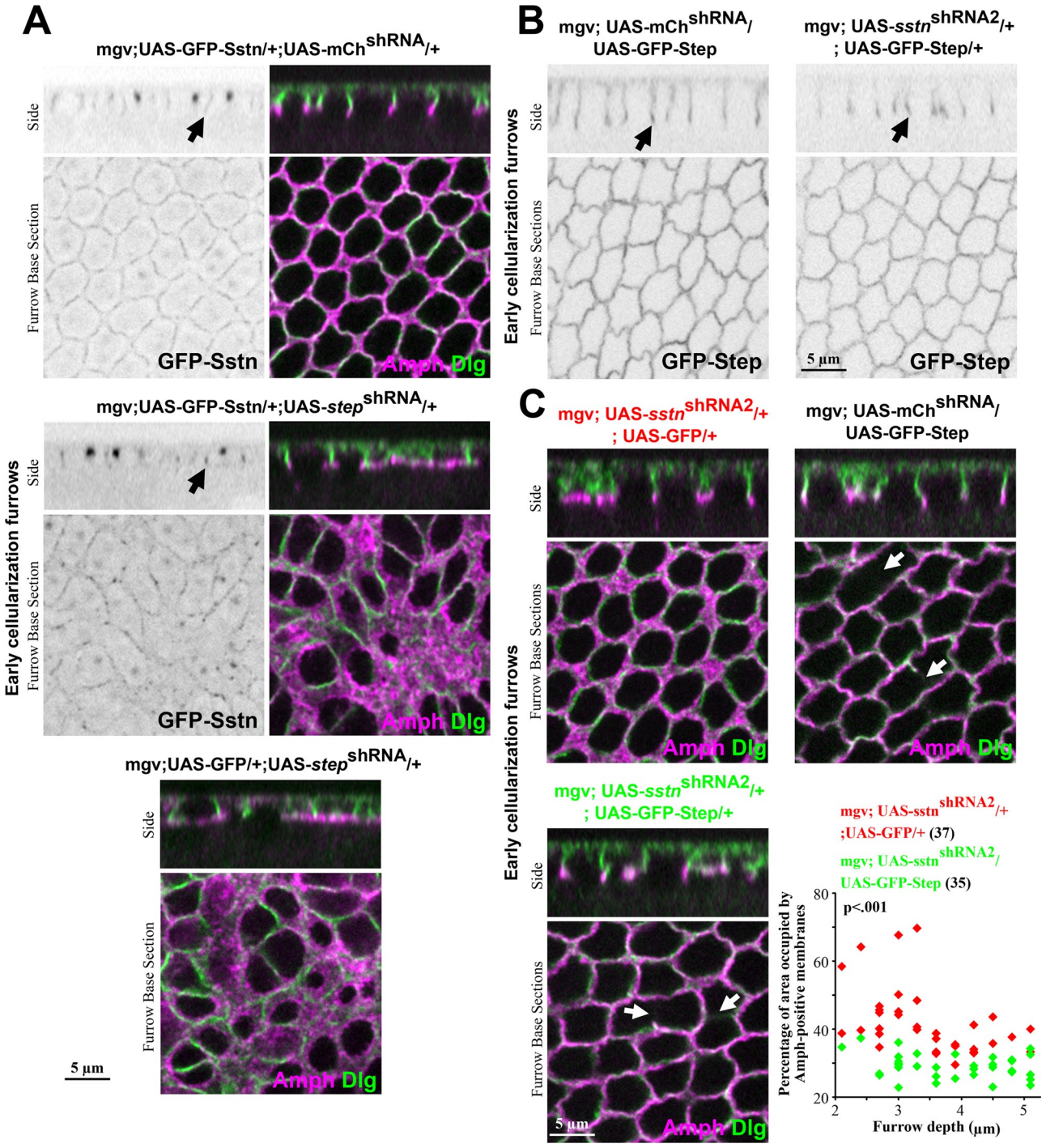


FIGURE 7: Step overexpression can overcome the effects of Sstn loss but not vice versa. (A) *step* shRNA had no apparent effect on GFP-Sstn localization to furrow membranes (arrows), and the localized GFP-Sstn had no apparent effect on the membrane expansion that occurs with Step loss (compare Amph staining). (B) *sstn* shRNA had no apparent effect on GFP-Step enrichment at basal furrow tips (arrows). (C) GFP-Step expression eliminated the furrow expansion that occurs with Sstn loss (quantified in graph as in Figure 5). Sporadic furrow loss is also observed in GFP-Step embryos that progress to early cellularization (arrows; 15 of 27 embryos were imaged with missing or shorter furrows at this stage) and was similarly seen in embryos with both GFP-Step and *sstn* shRNA expression (arrows; 22 of 52 embryos with missing or shorter furrows were imaged).

is coupled to an interaction with Par-3 at its C-terminal region to link cytohesin signaling to epithelial cell–cell junctions (Ikenouchi and Umeda, 2010), but *Drosophila* Par-3 (Bazooka) has no apparent effect on the basal tips of furrows in the early *Drosophila* embryo (Harris and Peifer, 2004).

In addition to Sstn, our data suggest that other positive regulators of Step localization and function are active in the early embryo. Specifically, despite high-level expression of three distinct shRNA constructs that reduced Sstn-GFP levels to below background levels, overexpressed Step-GFP could still localize to the membrane,

and the severity of membrane expansion with the loss of Sstn was never as strong at that with Step loss. A number of known cytohesin interactions can be considered as additional contributors to Step activities. First, the PH domains of cytohesins, and of Step, bind and respond to phosphoinositides (Chardin *et al.*, 1996; Klarlund *et al.*, 1997; Britton *et al.*, 2002). However, manipulations of PIP2 and PIP3 levels have no apparent effect on *Drosophila* pseudocleavage or early cellularization furrows, despite a strong effect on later cellularization furrows (Reversi *et al.*, 2014). Thus Step-PIP3 interactions may be dispensable or nonexistent at the furrow tips where Step acts. Second, the PH domains of cytohesins also bind and respond to GTP-bound Arf-like 4 (Arl4) and Arf small G proteins, forming recruitment pathways and positive feedback loops (Cohen *et al.*, 2007; Hofmann *et al.*, 2007; Li *et al.*, 2007; Stalder *et al.*, 2011), but these have not yet been examined for Step. Third, the Step CC domain mediates direct interactions with the adaptor CNK (Hahn *et al.*, 2013). To our knowledge, CNK has not been examined in the early embryo, but it is expressed (FlyBase). Although it was not detected with Step in our IP LC-MS analyses, it is possible that Step–CNK interactions might occur with the loss of Sstn. Fourth, the cytohesin CC domain can also mediate cytohesin homodimerization (DiNitto *et al.*, 2007, 2010), an interaction we detected for Step. Thus a lack of Step homodimerization with loss of its CC domain might explain why the Step CC domain deletion had greater effects on Step localization and function than with Sstn loss. With homodimerization capability, endogenous Step may be able to use additional activation mechanisms to elicit partial effects with Sstn loss, whereas with overexpression, Step can achieve greater localization and activity to make Sstn unnecessary. Although overexpressed Step can overcome the need for Sstn, it does have negative consequences (sporadic furrow loss). Thus Sstn may be needed to aid Step when it is expressed at lower, optimal, normal levels.

A recent study showed that FRMD4A is up-regulated in human squamous cell carcinoma and contributes to tumor growth and metastasis (Goldie *et al.*, 2012). Similarly, elevated cytohesin and Arf small G protein activities have also been shown to promote cancer progression (Hashimoto *et al.*, 2004; Tague *et al.*, 2004; Muralidharan-Chari *et al.*, 2009; Bill *et al.*, 2010; Fu *et al.*, 2014; Pan *et al.*, 2014). Thus elucidation of the roles and regulation of the Sstn (FRMD4A)–Step (cytohesin)–Arf small G protein axis during normal development should increase our understanding of such disease states. Specifically, improper pathway activity may lead to misregulation of the membrane cytoskeleton in other contexts, with potential downstream consequences for cell division, cell–cell adhesion, or cell migration.

## MATERIALS AND METHODS

### *Drosophila* genetics and molecular reagents

The Bloomington *Drosophila* Stock Center (BDSC; Bloomington, IN) provided $sstn^{Df(3L)BSC441}$ (BDSC #24945), $sstn^{EY06542}$ (BDSC #15826), and $rho1^{72O}$ (BDSC #7325) alleles, and the $sstn^{c04515}$ allele was from Exelixis at Harvard Medical School (Boston, MA). UAS constructs included UAS-GFP (gift from Ulrich Tepass, University of Toronto, Toronto, Canada), UAS-GFP-Step (Lee and Harris, 2013), UAS-GFP-$Step^{RNAi\text{-}resistant}$ (Lee and Harris, 2013), UAS-step-shRNA (BDSC #32374), UAS-mCh-shRNA (BDSC #35785), UAS-mCherry (BDSC#35787), and the constructs made in this study (see later description). UAS constructs were expressed maternally using maternal-α4-tubulin-GAL4-VP16 (mgv) (gift from Mark Peifer, University of North Carolina at Chapel Hill, Chapel Hill, NC) or the Maternal Triple Driver (MTD; BDSC #31777) or nos-GAL4 (BDSC#25751), and defects were assessed in offspring. In addition to the UAS-GFP line, a Histone-GFP line was also used as an internal staining control (gift from Andrew Wilde, University of Toronto).

The *sstn* shRNAs were designed based on the algorithm by Vert *et al.* (2006) and targeted three distinct sequences unique to *sstn*: shRNA1 top strand 5′-ctagcagtCAGCGACAACTAGATGCTATAtagttatattcaagcataTATAGCATCTAGTTGTCGCTGgcg-3′; shRNA2 top strand 5′-ctagcagtCGGCAACTACAAGCAACTCTAtagttatattcaagcataTAGAGTTGCTTGTAGTTGCCGgcg-3′; and shRNA3 top strand 5′-ctagcagtCACGATGAGATCTCACTGTCAtagttatattcaagcataTGACAGTGAGATCTCATCGTGgcg-3′. The constructs were ligated into the pValium22 vector (gift from the *Drosophila* Transgenic RNAi Resource Project) using the restriction enzymes *Nhe*1 and *Eco*R1, confirmed by PCR, sequenced, and targeted to the attp40 recombination site on chromosome 2 for transgenic flies (BestGene, Chino Hills, CA).

For GFP tagging, the *sstn* coding sequence was PCR amplified from cDNA (RE36140; *Drosophila* Genomics Resource Center, Bloomington, IN) using 5′-CGGGATCCCATGCAATTGAAAGCGCCCAAG-3′ (forward) and 5′-CCGCTCGAGTCAATTAGGATTTCCGCCCTC-3′ (reverse) primers and cloned into the pENTR vector using *Bam*HI and *Xho*I restriction sites. To delete the CC and CR regions, we synthesized DNA with the deletions (GeneScript, Piscataway, NJ) and cloned them into the pENTR vector using *Bam*HI and *Xho*I to create $Sstn^{\Delta CC}$ (deleting amino acids [aa] 60–133) and $Sstn^{\Delta CR}$ (deleting aa 587–627). Gateway cloning (Life Technologies, Burlington, Canada) recombined each construct into pPGW for N-terminal enhanced GFP tagging and placement downstream of the UASp promoter. An attb recombination site was cloned into the pPGW *Nsi*1 site. Vectors were targeted to the attp40 recombination site on chromosome2 (BestGene). For mCherry tagging, the full-length Sstn coding sequence from the same pENTR vector for GFP tagging was recombined into pPNTC (gift from Ulrich Tepass) for N-terminal mCherry tagging and placement downstream of the UASp promoter. The vector was targeted to the attp2 recombination site on chromosome 3. mCherry tagging of Step followed the same procedure but was targeted to attp40. For GFP-$Step^{\Delta CC}$, the CC region was deleted from *step* in the pENTR construct using 5′-GAATTCCCGGGTCGACTATGATTAGCGCAATGG-3′ (forward) and 5′-GTCAGTCAGTCACGAGCGGCCGCTATTAACTCTTG-3′ (reverse) primers and *Sal*I and *Not*I restriction enzymes. The mutagenesis was conducted with an established protocol (Lee and Harris, 2013) and confirmed by sequencing to create $Step^{\Delta CC}$ (deleting aa 31–70 of the 410-aa full-length sequence of isoform A). The construct was targeted to attp40.

All complex genotypes were synthesized using standard *Drosophila* genetics, and the presence of alleles and transgenes was confirmed after synthesis by probing for their expected phenotypes in single-disruption analyses.

### Immunoprecipitations and mass spectrometry

Embryos from 0.5 to 2.5 h were lysed with a Dounce homogenizer in 1% NP-40 buffer containing 50 mM 4-(2-hydroxyethyl)-1-piperazineethanesulfonic acid, 150 mM NaCl, 10% glycerol, 1.5 mM $MgCl_2$, 2 mM EDTA, 10 mM sodium pyrophosphate, 1 mM phenylmethylsulfonyl fluoride, 10 mM NaF, 0.25 mM $Na_3VO_4$, and protein inhibitor cocktail (Roche, Mississauga, Canada). After centrifugation, lysate supernatants were incubated with GFP-trap-A beads (ChromoTek, Martinsried, Germany) for 3 h. For Western blotting, proteins were eluted from the beads by boiling in 2× SDS–PAGE sample buffer with β-mercaptoethanol, separated by SDS–PAGE, and blotted. Blots were probed with antibodies against GFP (generated in our lab) or mCh (Abcam, Cambridge, UK). For LC-MS, proteins were eluted from the

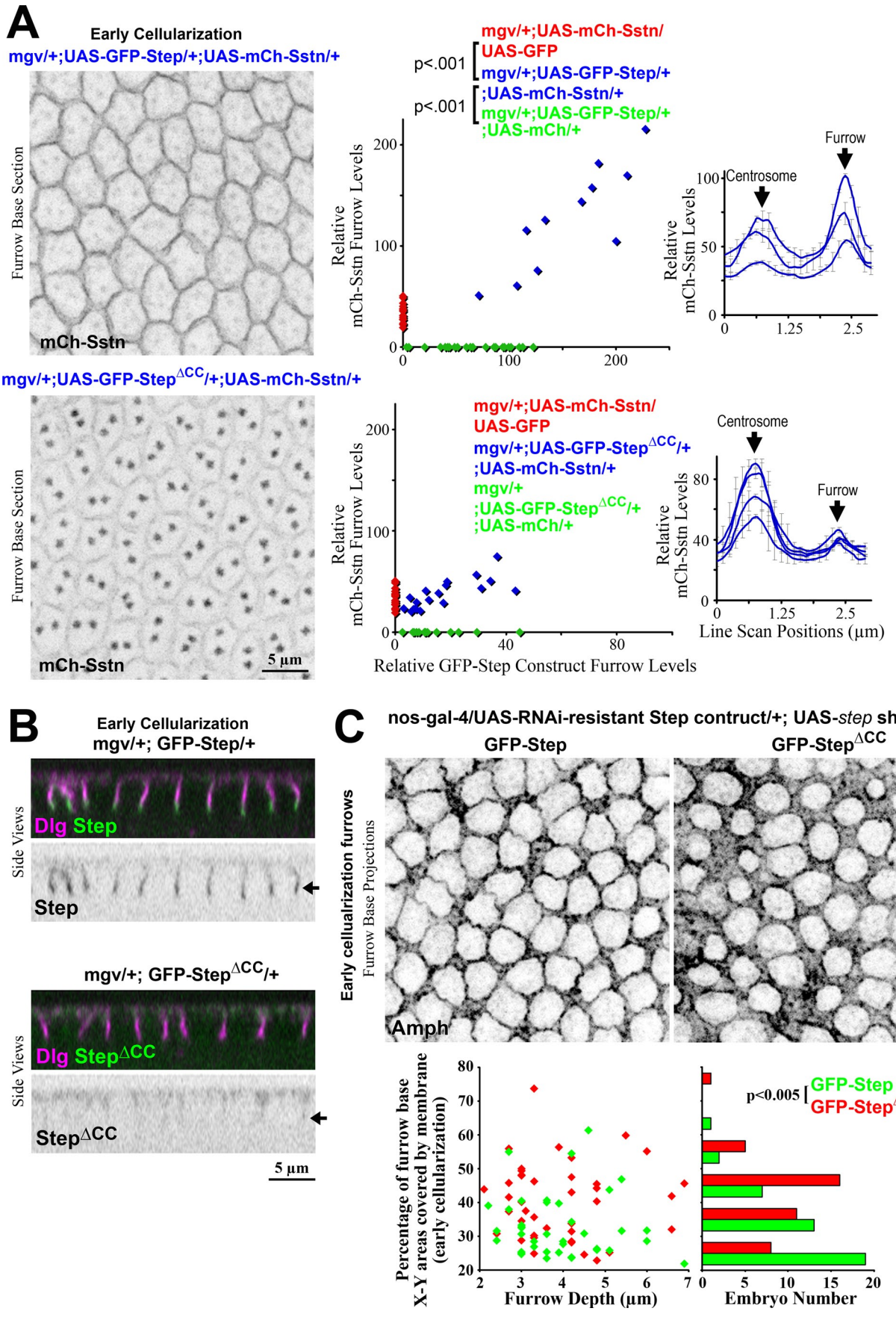


FIGURE 8: The Step coiled-coil domain is needed for Sstn association, Step localization and membrane growth restraint. (A) Furrow corecruitment of mCh-Sstn with GFP-Step but not GFP-Step$^{\Delta CC}$. In each case, images are shown after acquisition and adjustment with the same settings. Furrow levels were quantified as in Figure 3. Line scans were

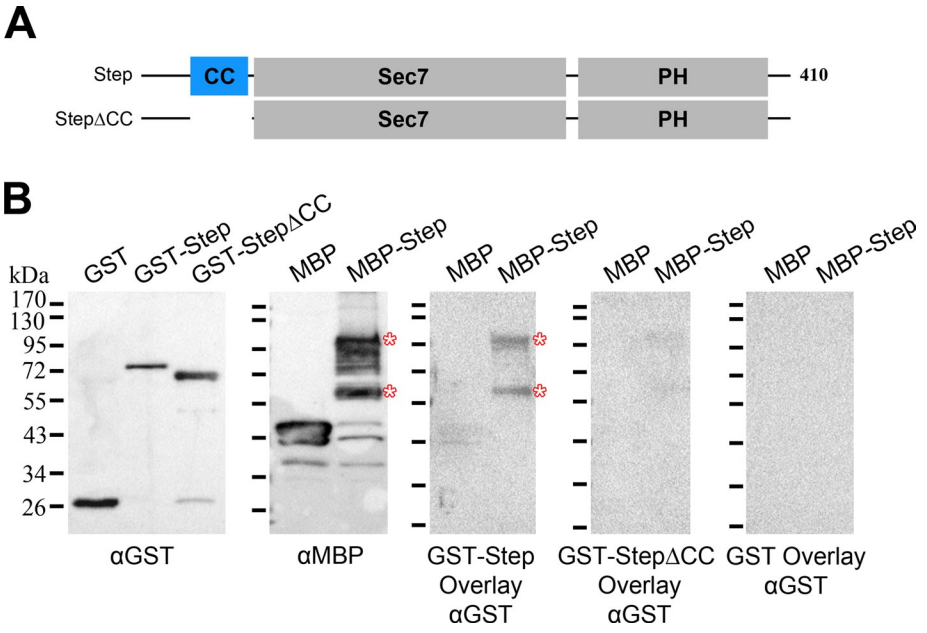


FIGURE 9: The Step coiled-coil domain mediates Step homodimerization. (A) Step constructs used in the binding assays. (B) Blot overlays showing binding of GST-Step to MBP-Step (asterisks) but not to higher levels of MBP. GST-Step$^{\Delta CC}$ showed much-reduced binding to MBP-Step, and GST showed no binding to MBP-Step, despite incubation of both at higher levels than GST-Step (see left blot for the relative GST, GST-Step, and GST-Step$^{\Delta CC}$ protein levels used for the overlays shown). The overlay blots were probed and imaged side by side with identical reagents and settings. The overall results were replicated in a separate complete analysis.

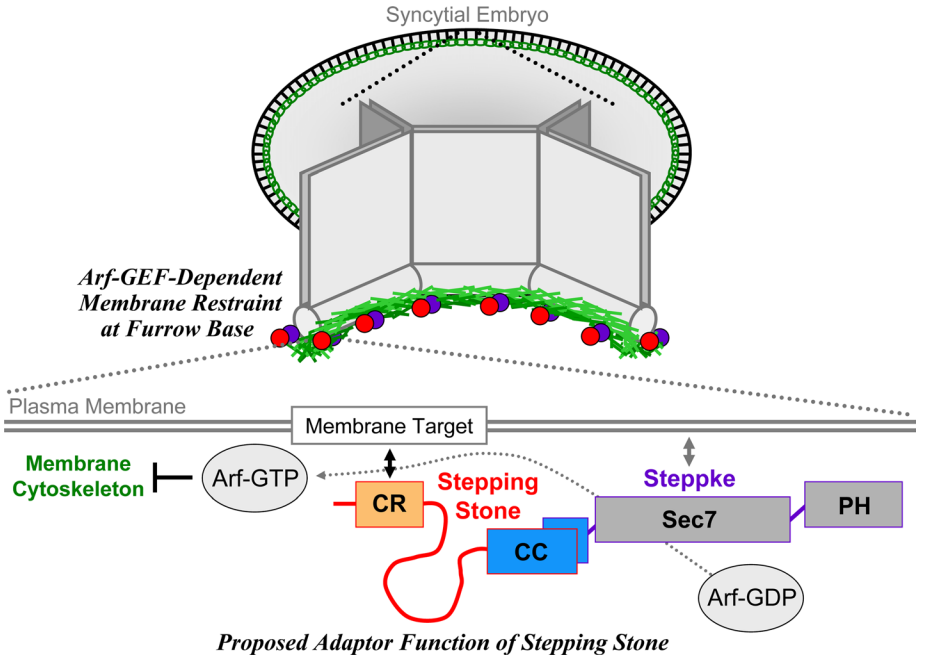


FIGURE 10: A model of Sstn as an adaptor for the promotion of Step-dependent membrane cytoskeleton restraint. See *Discussion* for details.

beads with 500 mM ammonium hydroxide at pH 11.0 (for GFP-Step) or treated further on the beads (for GFP-Sstn). The proteins were reduced in 10 mM dithiothreitol and alkylated using 30 mM iodoacetimide. The proteins were then directly digested with sequenced-grade trypsin (Promega, Madison, WI). Tryptic peptides were analyzed by LC-MS/MS using a linear ion trap mass spectrometer (model LTQ-XL; Thermo Fisher Scientific, Waltham, MA). The mass spectrometer was operated and the output was analyzed as described previously (Ahmed *et al.*, 2012).

### Blot overlays and molecular reagents

A 1- to 3-µg amount of each MBP fusion protein was fractionated by 10% SDS–PAGE and transferred to nitrocellulose. The blots were blocked with 5% milk dissolved in TBST buffer (8.0 g of NaCl, 2.42 g of Tris, and 1 ml of Tween-20 in 1 l of double-distilled $H_2O$, pH adjusted to 8.0), incubated with ~7 µg of each GST fusion protein in TBST buffer with 5% milk, washed, incubated with GST antibodies (generated in our lab) in TBST buffer with 5% milk, washed, incubated with horseradish peroxidase–conjugated goat anti-rabbit antibodies, washed, and then exposed to chemiluminescent reagents (Thermo Fisher Scientific) and imaged with a Chemi-Doc XRS (Bio-Rad, Hercules, CA). The proteins were also individually evaluated using the GST antibodies and MBP antibodies (NEB, Whitby, Canada). Before each final binding assay, we adjusted the amounts of each protein on the blots or in solution so that control or noninteracting proteins were always present at higher molar levels than those that interacted (based on GST or MBP staining of diagnostic Western blots).

For MBP-Sstn, the Sstn coding sequence was subcloned from the pENTR construct using 5′-CGGGATCCATGCAATTGAAAGCGCCCAAGAGCAGAAATATG-3′ (forward) and 5′-CCCAAGCTTTCAATTAGGATTTCCGCCCTCCTTTTGCTTAAAC-3′ (reverse) primers and cloned into pMAL-2X vector with *Bam*HI and *Hin*dIII. For MBP-Sstn$^{\Delta CC}$, the Sstn$^{\Delta CC}$ sequence was amplified from the synthesized clone using 5′-AACTGCAGATGCAATTGAAAGCGCCCAAGAGCAGAAATATG-3′ (forward) and 5′-CCCAAGCTTTCAATTAGGATTTCCGCCCTCCTTTTGCTTAAAC-3′ (reverse) primers and

performed as in Figure 3. The overall relationships were reproduced with an independent set of crosses. (B) GFP-Step displays enrichment at the base of furrows, but GFP-Step$^{\Delta CC}$ does not (arrows). Dlg shows cellularization furrows of similar depth. (C) Expression of an RNAi-resistant GFP-Step construct with *step* shRNA restrains perpendicular membrane expansion at the base of furrows (marked with Amph) more effectively than expression of RNAi-resistant GFP-Step$^{\Delta CC}$. Quantifications of furrow base areas in the *xy*-plane are shown for embryos with 2- to 7-µm-deep furrows and were performed as in Figure 5. Each point in the left graph is one embryo measurement. The right graph compiles all of these points into a histogram.

cloned into pMAL-2X vector with *Pst*I and *Hin*dIII. For GST-Step, the *step* coding sequence was subcloned from a pENTR construct (Lee and Harris, 2013) into the pGEX-6P-2 vector using 5′-CGGGATCCATGCAATTGAAAGCGCCCAAG-3′ (forward) and 5′-CCGCTCGAGTCAATTAGGATTTCCGCCCTC-3′ (reverse) primers and *Bam*HI and *Xho*I restriction enzymes. For GST-Step$^{\Delta CC}$, the pENTR vector deletion construct used for GFP-tagging was used for subcloning, as done for full length. For MBP-Step, the *step* coding sequence was subcloned from the pENTR construct into the pMAL-2X vector using 5′-CGGGATCCATGATTAGCGCAATGGACAATTTCG-3′ (forward) and 5′-AACTGCAGTTAACTCTTGCTGAGTGCCTTTTTC-3′ (reverse) primers and *Bam*HI and *Pst*I restriction enzymes.

### Embryo staining and imaging

Embryos were fixed for 20 min in 1:1 3.7% formaldehyde in phosphate-buffered saline (PBS):heptane and then devitellinized in methanol. Blocking and staining were in PBS containing 1% goat serum, 0.1% Triton X-100, and 1% sodium azide. Antibodies used were as follows: rabbit, amphiphysin (1:2000; gift of Gabrielle Boulianne, Hospital for Sick Children, Toronto, Canada), Nup-50 (1:35,000; gift of J. Grosshans, Institute of Biochemistry and Molecular Cell Biology, Göttingen, Germany); mouse, Dlg (1:100; Developmental Studies Hybridoma Bank [DSHB], Iowa City, IA), and Peanut (1:10; DSHB). Secondary antibodies were conjugated to Alexa Fluor 488, Alexa Fluor 546, and Alexa Fluor 647 (Invitrogen). Embryos were mounted in Aqua Polymount (Polysciences, Warrington, PA).

Images were collected by a spinning disk confocal system (Quorum Technologies, Guelph, Canada) at room temperature using a 63× Plan Apochromat numerical aperture 1.4 objective (Carl Zeiss, Toronto, Canada) with a piezo top plate and an electron-multiplying charge-coupled device camera (Hamamatsu Photonics, Hamamatsu, Japan). *Z*-stacks had 300-nm step sizes. Images were analyzed with Volocity software (PerkinElmer, Waltham, MA) and ImageJ (National Institutes of Health, Bethesda, MD) as indicated in the figures and figure legends. Images were deconvolved using the Volocity Restoration tool with 15 iterations or a confidence of >95% (the first one achieved).

Photoshop (Adobe) and ImageJ were used for figure preparation. Except where noted, input levels were adjusted so that the main signal range spanned the entire output grayscale. Images were resized by bicubic interpolation without noticeable changes at normal viewing magnifications.

### Sequence analyses

Coiled-coils were predicted using Coils (scores >0.500) and Marcoil (scores >50%). Searches of other species sequences were conducted with blastp (National Center for Biotechnology Information). Multiple alignments were generated with T-Coffee and verified with pairwise blastp results.

### Statistics

Comparisons were done using Student's *t* tests. Means are shown with SD.

## ACKNOWLEDGMENTS

We thank R. Winklbauer for critiquing the manuscript and G. Boulianne, U. Tepass, M. Peifer, A. Wilde, and the *Drosophila* Transgenic RNAi Resource Project for reagents. The work was supported by a Canadian Institutes of Health Research operating grant to T.H. (MOP82829). T.H. also holds a Tier 2 Canada Research Chair.

## REFERENCES

Ahmed SM, Theriault BL, Uppalapati M, Chiu CW, Gallie BL, Sidhu SS, Angers S (2012). KIF14 negatively regulates Rap1a-Radil signaling during breast cancer progression. J Cell Biol 199, 951–967.

Bill A, Schmitz A, Albertoni B, Song JN, Heukamp LC, Walrafen D, Thorwirth F, Verveer PJ, Zimmer S, Meffert L, *et al*. (2010). Cytohesins are cytoplasmic ErbB receptor activators. Cell 143, 201–211.

Bos JL, Rehmann H, Wittinghofer A (2007). GEFs and GAPs: critical elements in the control of small G proteins. Cell 129, 865–877.

Britton JS, Lockwood WK, Li L, Cohen SM, Edgar BA (2002). Drosophila's insulin/PI3-kinase pathway coordinates cellular metabolism with nutritional conditions. Dev Cell 2, 239–249.

Chardin P, Paris S, Antonny B, Robineau S, Beraud-Dufour S, Jackson CL, Chabre M (1996). A human exchange factor for ARF contains Sec7- and pleckstrin-homology domains. Nature 384, 481–484.

Cherfils J, Zeghouf M (2013). Regulation of small GTPases by GEFs, GAPs, and GDIs. Physiol Rev 93, 269–309.

Cohen LA, Honda A, Varnai P, Brown FD, Balla T, Donaldson JG (2007). Active Arf6 recruits ARNO/cytohesin GEFs to the PM by binding their PH domains. Mol Biol Cell 18, 2244–2253.

DiNitto JP, Delprato A, Gabe Lee MT, Cronin TC, Huang S, Guilherme A, Czech MP, Lambright DG (2007). Structural basis and mechanism of autoregulation in 3-phosphoinositide-dependent Grp1 family Arf GTPase exchange factors. Mol Cell 28, 569–583.

DiNitto JP, Lee MT, Malaby AW, Lambright DG (2010). Specificity and membrane partitioning of Grsp1 signaling complexes with Grp1 family Arf exchange factors. Biochemistry 49, 6083–6092.

Donaldson JG, Jackson CL (2011). ARF family G proteins and their regulators: roles in membrane transport, development and disease. Nat Rev Mol Cell Biol 12, 362–375.

D'Souza-Schorey C, Chavrier P (2006). ARF proteins: roles in membrane traffic and beyond. Nat Rev Mol Cell Biol 7, 347–358.

Fu Y, Li J, Feng MX, Yang XM, Wang YH, Zhang YL, Qin W, Xia Q, Zhang ZG (2014). Cytohesin-3 is upregulated in hepatocellular carcinoma and contributes to tumor growth and vascular invasion. Int J Clin Exp Pathol 7, 2123–2132.

Fuss B, Becker T, Zinke I, Hoch M (2006). The cytohesin Steppke is essential for insulin signalling in Drosophila. Nature 444, 945–948.

Gillingham AK, Munro S (2007). The small G proteins of the Arf family and their regulators. Annu Rev Cell Dev Biol 23, 579–611.

Goldie SJ, Mulder KW, Tan DW, Lyons SK, Sims AH, Watt FM (2012). FRMD4A upregulation in human squamous cell carcinoma promotes tumor growth and metastasis and is associated with poor prognosis. Cancer Res 72, 3424–3436.

Hahn I, Fuss B, Peters A, Werner T, Sieberg A, Gosejacob D, Hoch M (2013). The Drosophila Arf GEF Steppke controls MAPK activation in EGFR signaling. J Cell Sci 126, 2470–2479.

Harris TJ, Peifer M (2004). Adherens junction-dependent and -independent steps in the establishment of epithelial cell polarity in Drosophila. J Cell Biol 167, 135–147.

Hashimoto S, Onodera Y, Hashimoto A, Tanaka M, Hamaguchi M, Yamada A, Sabe H (2004). Requirement for Arf6 in breast cancer invasive activities. Proc Natl Acad Sci USA 101, 6647–6652.

Hofmann I, Thompson A, Sanderson CM, Munro S (2007). The Arl4 family of small G proteins can recruit the cytohesin Arf6 exchange factors to the plasma membrane. Curr Biol 17, 711–716.

Ikenouchi J, Umeda M (2010). FRMD4A regulates epithelial polarity by connecting Arf6 activation with the PAR complex. Proc Natl Acad Sci USA 107, 748–753.

Kitano J, Kimura K, Yamazaki Y, Soda T, Shigemoto R, Nakajima Y, Nakanishi S (2002). Tamalin, a PDZ domain-containing protein, links a protein complex formation of group 1 metabotropic glutamate receptors and the guanine nucleotide exchange factor cytohesins. J Neurosci 22, 1280–1289.

Klarlund JK, Guilherme A, Holik JJ, Virbasius JV, Chawla A, Czech MP (1997). Signaling by phosphoinositide-3,4,5-trisphosphate through proteins containing pleckstrin and Sec7 homology domains. Science 275, 1927–1930.

Lee DM, Harris TJ (2013). An Arf-GEF regulates antagonism between endocytosis and the cytoskeleton for Drosophila blastoderm development. Curr Biol 23, 2110–2120.

Lee DM, Harris TJ (2014). Coordinating the cytoskeleton and endocytosis for regulated plasma membrane growth in the early embryo. Bioarchitecture 4, 68–74.

Li CC, Chiang TC, Wu TS, Pacheco-Rodriguez G, Moss J, Lee FJ (2007). ARL4D recruits cytohesin-2/ARNO to modulate actin remodeling. Mol Biol Cell 18, 4420–4437.

Lim J, Zhou M, Veenstra TD, Morrison DK (2010). The CNK1 scaffold binds cytohesins and promotes insulin pathway signaling. Genes Dev 24, 1496–1506.
Muralidharan-Chari V, Hoover H, Clancy J, Schweitzer J, Suckow MA, Schroeder V, Castellino FJ, Schorey JS, D'Souza-Schorey C (2009). ADP-ribosylation factor 6 regulates tumorigenic and invasive properties in vivo. Cancer Res 69, 2201–2209.
Nevrivy DJ, Peterson VJ, Avram D, Ishmael JE, Hansen SG, Dowell P, Hruby DE, Dawson MI, Leid M (2000). Interaction of GRASP, a protein encoded by a novel retinoic acid-induced gene, with members of the cytohesin family of guanine nucleotide exchange factors. J Biol Chem 275, 16827–16836.
Pan T, Sun J, Hu J, Hu Y, Zhou J, Chen Z, Xu D, Xu W, Zheng S, Zhang S (2014). Cytohesins/ARNO: the function in colorectal cancer cells. PLoS One 9, e90997.
Reversi A, Loeser E, Subramanian D, Schultz C, De Renzis S (2014). Plasma membrane phosphoinositide balance regulates cell shape during Drosophila embryo morphogenesis. J Cell Biol 205, 395–408.
Rosenbaum DM, Rasmussen SG, Kobilka BK (2009). The structure and function of G-protein-coupled receptors. Nature 459, 356–363.
Stalder D, Barelli H, Gautier R, Macia E, Jackson CL, Antonny B (2011). Kinetic studies of the Arf activator Arno on model membranes in the presence of Arf effectors suggest control by a positive feedback loop. J Biol Chem 286, 3873–3883.
Tague SE, Muralidharan V, D'Souza-Schorey C (2004). ADP-ribosylation factor 6 regulates tumor cell invasion through the activation of the MEK/ERK signaling pathway. Proc Natl Acad Sci USA 101, 9671–9676.
Torii T, Miyamoto Y, Sanbe A, Nishimura K, Yamauchi J, Tanoue A (2010). Cytohesin-2/ARNO, through its interaction with focal adhesion adaptor protein paxillin, regulates preadipocyte migration via the downstream activation of Arf6. J Biol Chem 285, 24270–24281.
Vert JP, Foveau N, Lajaunie C, Vandenbrouck Y (2006). An accurate and interpretable model for siRNA efficacy prediction. BMC Bioinformatics 7, 520.
Zhu W, London NR, Gibson CC, Davis CT, Tong Z, Sorensen LK, Shi DS, Guo J, Smith MC, Grossmann AH, *et al*. (2012). Interleukin receptor activates a MYD88-ARNO-ARF6 cascade to disrupt vascular stability. Nature 492, 252–255.